photonics

MDPI

Article

On the Possibility of Intense Unipolar THz Pulses Formation in Nonhomogeneous Nonequilibrium Nitrogen Plasma Channels

Anna V. Bogatskaya [1,2,*], Ekaterina A. Volkova [3] and Alexander M. Popov [1,2]

[1] Department of Physics, Moscow State University, 119991 Moscow, Russia
[2] P. N. Lebedev Physical Institute, RAS, 119991 Moscow, Russia
[3] D. V. Skobeltsyn Institute of Nuclear Physics, Moscow State University, 119991 Moscow, Russia
* Correspondence: abogatskaya@mics.msu.su

Abstract: We developed a 3D, fully self-consistent model for analysis of the ultrashort THz unipolar pulse formation accompanied by its amplification in a nonequilibrium plasma channel induced in nitrogen by a femtosecond UV laser pulse. The model is based on a self-consistent numerical solution of the second-order wave equation in cylindrical geometry and the kinetic Boltzmann equation for the electron velocity distribution function (EVDF) at different points of the spatially inhomogeneous nonequilibrium plasma channel. Rapid relaxation of the electron velocity distribution function in the plasma channel results in the amplification of the leading front of the THz pulse only, while its trailing edge is not amplified or even absorbed, which gives rise to the possibility of the formation of pulses with a high degree of unipolarity. The evolution of the unipolar pulse after its transfer from the channel to open free space is analyzed in detail.

Keywords: unipolar pulses; terahertz generation in plasma; Boltzmann kinetic equation; nonequilibrium plasma; self-consistent numerical modeling

Citation: Bogatskaya, A.V.; Volkova, E.A.; Popov, A.M. On the Possibility of Intense Unipolar THz Pulses Formation in Nonhomogeneous Nonequilibrium Nitrogen Plasma Channels. *Photonics* **2023**, *10*, 113. https://doi.org/10.3390/photonics10020113

Received: 27 December 2022
Revised: 18 January 2023
Accepted: 19 January 2023
Published: 21 January 2023

1. Introduction

The problem of the generation of extremely short electromagnetic pulses or so-called (quasi) unipolar pulses with the non-zero value of the electric pulse area is widely studied nowadays [1–4]. Really, the practical importance of unipolar pulses, in contrast to the usual bipolar pulses containing several cycles of oscillations, lies in their ability to have a unidirectional impact on charged particles which makes it possible to nonresonantly excite quantum systems over shorter times [2,5–7], accelerate free charges [8–10], control molecular orientation and alignment [11,12] and a lot of other applications [see the review [13] and references therein]. However, it is known that when unipolar pulses propagate in empty space or are focused, the unipolarity is lost [14,15]. This fact often casts doubt on the prospects of the practical use of unipolar pulses for exploring problems related to the action of unipolar pulses on some remote target. Accordingly, the main purpose of this paper is to demonstrate the possibility of keeping the unipolarity at some distances during the pulse propagation, even in free space. We provide rigorous 3D calculations showing the unipolar pulse formation while propagating a one-cycle THz pulse in a cylindrical nonequilibrium plasma channel in air, as well as its evolution after exiting the plasma channel into free space. The obtained results will make it possible to determine at what distances targets can be placed to observe the unique features of unipolar pulses.

Unipolar pulses were introduced for the first time in [16]. Even then, the question was acute if such pulses could propagate in free space. From one point of view, a unipolar pulse has the non-zero static electric field component and hence cannot propagate in space. On the other hand, it is well known that any function $f(x,t) = f(x \mp ct)$ of the

retarded/leading argument $\zeta = x \mp ct$ represents the solution of the second-order wave equation

$$\frac{\partial^2 f(x,t)}{\partial x^2} = \frac{1}{c^2}\frac{\partial^2 f(x,t)}{\partial t^2} \quad (1)$$

For the case of electromagnetic signal f stands for the electric field strength and c is the speed of light in vacuum or in nondispersive media. Evidently, the integral of the pulse area

$$S = \int f(x,t)dx = c\int f(x,t)dt = const \quad (2)$$

That was first introduced in [16,17] can have any non-zero value, both positive or negative. The 3D generalization of the pulse electric field area was given in [18] as

$$S(t) = \int E(\rho,z,t)\rho d\rho dz. \quad (3)$$

Further, we introduce the unipolar factor as the normalized pulse electric field area:

$$U(t) = \int E(\rho,z,t)\rho d\rho dz / \int |E(\rho,z,t)|\rho d\rho dz. \quad (4)$$

We believe that the one-dimensional wave Equation (1) can be used at least at distances less the diffraction length $\Lambda = kR_0^2$, where R_0 is the beam transverse size and $k = 2\pi/\lambda$ is the wave number, λ is the wavelength. The diffraction length is different for different pulse spectral components, and it is infinitely small for the static field. Further, we will demonstrate that this fact leads to the decrement of the absolute value of the unipolar factor in time upon propagation of such a pulse in free space. Nevertheless, the *U*-factor will maintain its nonzero value during some time intervals. A more complicated situation appears to exist in nonequilibrium and inhomogeneous media suitable for the generation of the pulses with the non-zero *U*-factors.

At present, a number of methods to produce subcycle unipolar pulse in different frequency ranges from THz to UV have been proposed [1–4,18–24]. In particular, in [22], the possibility to transform the single-cycle THz pulse to the unipolar one during the process of its propagation in the extended nonequilibrium xenon plasma channel with a peak-like electron velocity distribution function (EVDF) was demonstrated. Such a channel can be formed by multiphoton ionization of xenon by the femtosecond UV laser pulse and used for amplification of THz radiation [25,26]. It is important that the position of the photoelectron peak should be in the energy range with a growing transport cross-section. We remind that only the frequency band below the electron transport frequency can be amplified in such a plasma. The mechanism of amplification is discussed in detail in recent papers [25–27]. If the intensity of the amplified pulse is strong enough, the time of the peak–like EVDF relaxation becomes less than the pulse duration, which results in the dominant amplification of the leading part of the pulse compared to the trailing edge, so the pulse evolves to the unipolar one [18].

Nitrogen molecules are also characterized by the energy interval with the growing transport cross-section [28]. Hence the air (nitrogen) plasma channel can be used for the amplification of THz radiation as well. Such a possibility was demonstrated in [29].

In this paper, we develop the 3D consideration of the recently proposed method to generate unipolar THz pulses in extended nonequilibrium air (or nitrogen) plasma channels [27]. The conducted research enables us to analyze the impact of pulse diffraction on the unipolarity degree as well as the importance of practical applications problem of transferring a unipolar signal from a plasma channel. The study is based on a joint solution of the second-order wave equation in cylindrical geometry for the nearly linear-polarized THz field and the set of kinetic Boltzmann equations in the two-term expansion for each spatial point of the plasma channel. The inverse effect of the amplified THz field on plasma evolution is rigorously calculated.

It is important to note that the excitation of low-energy vibrational states of N2 molecules makes the relaxation of the initial peak-like EVDF at least three orders of magnitude faster than in Xe. As a result, for atmospheric pressure, only pulses of several picoseconds can be amplified [29,30]. In this case, the transformation of a single-cycle THz pulse to the unipolar one can be achieved at any value of pulse energy. We also analyze for the first time the problem of transferring of unipolar THz pulse formed in the plasma channel into nonionized gas (or vacuum). This study is of great importance for a lot of practical applications since, in future experiments, it will be necessary to deliver a unipolar pulse from the plasma channel to the remote target.

2. 3D Model

According to our model, the femtosecond UV laser pulse propagates in air (at atmospheric pressure) along the z-direction and produces an extended plasma channel via multiphoton ionization. For oxygen molecules (ionization potential $I_i \approx 12.08$ eV) ionized by the third harmonic of Ti-Sa laser ($\hbar\Omega \approx 4.65$ eV), the photoelectron peak will be at the energy $\varepsilon_0 = 3\hbar\Omega - I_i \approx 1.87$ eV. This energy value appears to be approximately in the middle of the rather narrow energy interval 1.7 – 2.2 eV ($\sim 7.0 \cdot 10^7 - 8.0 \cdot 10^7$ cm/s) of increasing transport cross-section of N_2 molecules $\sigma_{tr}(v)$ (see Figure 1). As for nitrogen molecules (ionization potential 15.58 eV), one needs four photons for ionization. For moderate fields with the laser intensity ~10^{12} W/cm^2 in accordance with the perturbation theory, the probability of three-photon ionization is significantly larger than the four-photon one. Hence, the plasma channel is mainly produced by the three-photon ionization of O_2 molecules.

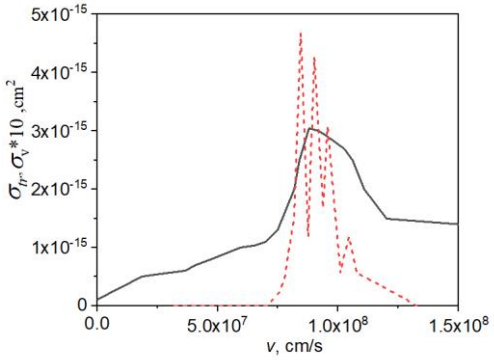

Figure 1. Transport cross-section (solid line) and cross-section of the vibrational level excitation $\sigma_v^{(1)}(v)$ $X\ ^1\Sigma, v = 1$ (dashed line) for the N_2 molecule. The plot is based on data from [26].

The formed photoionized plasma can be considered as a medium for radiation amplification according to the mechanism proposed in [25,26]. We note that in contrast to rare gases, the vibrational excitation leads to the rather rapid relaxation of the photoelectron peak [29]. The cross-section for excitation of the lowest vibrational state of an N_2 molecule is plotted in Figure 1. The vibrational cross section grows up rapidly for the absolute values of electron velocities above 7.5×10^7cm/s (~1.7 eV). This fact additionally reduces the desirable initial energy of the photoelectron peak for the effective amplification of the THz radiation. On the other hand, rapid relaxation of the EVDF in photoionized nitrogen plasma makes the length of amplification behind the leading UV pulse quite narrow, so only extremely short THz pulses (up to single-cycle and even unipolar ones) can be generated in such channels.

Further, we assume that the THz pulse propagates behind the UV femtosecond pulse, being located in its amplifying zone. We also suppose that the ionizing femtosecond pulse propagates through the gas at the speed of light.

The radial profile of electrons in the plasma channel formed by the UV pulse is chosen to be Gaussian-shaped.

$$N_e = N_e^{(0)}(z) \times exp(-(\rho/R_0)^2). \quad (5)$$

Here $N_e^{(0)}(z)$ is an on-axis profile of the electron density in the channel and R_0 stands for the channel radius. We consider different distributions of the electron density along z-axis. One of them is the sharp rectangular profile:

$$N_e^{(0)}(z) = \begin{cases} N_0, & z < L, \\ 0, z > L. \end{cases} \quad (6)$$

Here L is the length of the channel created due to ionization by the UV pulse. Such a profile does not look very realistic but allows us to emphasize the salient features of transferring extremely short (and first of all unipolar) THz pulses from the plasma channel to the surrounding non-ionized gas.

Another profile of the electron density accounts for the smoothing of the rectangular form (6):

$$N_e^{(0)}(z) = \begin{cases} N_0, & z < L - \delta/2, \\ 0.5 \times N_0 \left(1 + sin\dfrac{\pi(L-z)}{2\delta}\right), & L - \delta/2 < z < L + \delta/2, \\ 0, z > L + \delta/2. \end{cases} \quad (7)$$

Here δ is the thickness of the transition layer between the plasma and nonionized gas. In our simulations, we neglect the decrement of the UV radiation intensity due to its absorption in the plasma channel. Such absorption results from UV energy losses in the process of multiphoton ionization of molecules inside the channel. For typical UV pulse parameters (intensity ~10^{12}–10^{13} W/cm^2, pulse duration ~100 fs) that are necessary to form the channel with electron density up to 10^{14} cm^{-3} the propagation length will be much larger than the spatial size $L = 30$ cm which is considered below.

To study the propagation and amplification of ultrashort bipolar or unipolar THz pulses similar to [18] we solve the second-order wave equation for the nearly linear polarized field in cylindrical geometry (z-axis is directed along the propagation of UV and THz pulses):

$$\frac{\partial^2 E}{\partial z^2} + \frac{1}{\rho}\frac{\partial}{\partial \rho}\left(\rho \frac{\partial E}{\partial \rho}\right) = \frac{1}{c^2}\frac{\partial^2 E}{\partial t^2} + \frac{4\pi}{c^2}\frac{\partial j}{\partial t} \quad (8)$$

Here $\vec{r} = \{\rho, z\}$ is the radius-vector, $E(\rho, z, t)$ is the electric field strength, $j(\rho, z, t)$ is the current density induced by the THz pulse. This current was calculated on the basis of the Boltzmann kinetic equation. The general approach to calculate this current in nonequilibrium partially ionized plasma for arbitrary electromagnetic pulse duration (including extremely short single or subcycle pulses) is discussed in [31,32].

By analogy with [16,30], the wave equation was solved numerically on the grid moving with the leading UV pulse so the last is in the point $z - ct = 0$ at any instant of time. Hence, the amplified THz pulse is always in the range of negative coordinates.

The seed THz pulse is supposed to have the Gaussian envelope

$$E(z, \rho, 0) = E_0 \times exp(-(\rho/\rho_0)^2) \times$$

$$\times exp\left(-\frac{1}{2}\left((z - z_0)/z_p\right)^2\right) \times \left(cos\left(\frac{\omega_0 z}{c}\right) - sin\left(\frac{\omega_0 z}{c}\right) \times \left(\frac{z - z_0}{z_p}\right)\right) \quad (9)$$

Here E_0 is the amplitude value of the electric field, ω_0 is the carrier pulse angular frequency, ρ_0 is the pulse transverse radius, z_p is the half-pulse duration in the spatial domain and z_0 is the position of the pulse "center of mass" relative to the leading UV pulse. It is important to note that the given expression provides zero value of the pulse square, i.e.,

$$\int E(\rho,z)\rho d\rho dz = 0. \quad (10)$$

Hereafter, we assume that the plasma channel and seed THz pulse transverse radii are equal $\rho_0 = R_0$ and $\omega_0 = 2\times10^{12}$ s^{-1}. Two values, namely 1.0 and 1.5 cm are taken for the plasma channel radii. The parameter z_p is chosen $z_p = 0.025$ cm, that corresponds to the seed half-pulse duration $\tau_p = z_p/c \approx 8.38\times10^{-13}$ s. The pulse initial position was $z_0 = -5z_p \approx -0.125$ cm. For the above parameters the pulse given by (9) is nearly a single cycle pulse. Such pulse shapes are rather typical for modern experiments [23,33,34]. Also, it is important that the plasma channel radius is much greater than the seed THz pulse wavelength $\lambda = 2\pi c/\omega_0$.

To calculate the current in the right side of Equation (8) one needs to find the electron velocity distribution function (EVDF). In analogy with [18] the EVDF was calculated from the Boltzmann equation in the two-term expansion [35,36]:

$$f(\vec{r},\vec{v},t) = f_0(\vec{r},v,t) + \cos\vartheta\, f_1(\vec{r},v,t), \quad (11)$$

(Here ϑ is the angle between the electron velocity and electric field strength vectors) where the zero-order harmonic $f_0(\vec{r},v,t)$ stands for the distribution over the absolute value of velocity, while the first-order one $f_1(\vec{r},v,t)$ provides the possibility to calculate the current density:

$$j(\vec{r},t) = -\frac{4\pi e N_e(\vec{r})}{3}\int v^3 f_1(\vec{r},v,t)dv. \quad (12)$$

The two-term expansion set of equations for EVDF harmonics reads [35]:

$$\frac{\partial f_0(\vec{r},v,t)}{\partial t} = \frac{eE(\vec{r},t)}{3mv^2}\frac{\partial}{\partial v}\left(v^2 f_1(\vec{r},v,t)\right) + \frac{m}{M}\frac{1}{v^2}\frac{\partial}{\partial v}\left(\nu_{tr}(v)\left(vf_0 + \frac{T_g}{m}\frac{\partial f_0}{\partial v}\right)\right) + Q^*(f_0), \quad (13)$$

$$\frac{\partial f_1(\vec{r},v,t)}{\partial t} + \nu_{tr}(v) f_1(\vec{r},v,t) = \frac{eE(\vec{r},t)}{m}\frac{\partial f_0(\vec{r},v,t)}{\partial v}. \quad (14)$$

and $\nu_{tr}(v) = N\sigma_{tr}(v)v$ is the transport cross section, $N = 2.5\times10^{19}$ cm^{-3} is the gas density. In comparison with [18] here there is the inelastic collisional integral Q^* that leads to rapid (in picosecond time scale) relaxation of the EVDF in the nitrogen plasma channel. As a result, the possibility to produce pulses with a nonzero integral U appears to exist for low-intensity THz pulse as well.

The collisional integral Q^* was taken in a form [27]

$$Q_0^{(inel)} = -N\sum_i(\sigma_i^*(v)vf_0(x,v,t) + \sigma_i^*(V)Vf_0(x,V,t)(V/v)). \quad (15)$$

Here $\sigma_i^*(v)$ is the vibrational excitation cross section of the i-th vibrational level of the $N_2(X\,^1\Sigma,v)$ with the threshold $I_i^{(v)}$, velocity V can be expressed through v via the relation:

$$\frac{mV^2}{2} = \frac{mv^2}{2} + I_i^{(v)}, \quad (16)$$

Eight lower vibrational excitation cross-sections were taken into account. The thresholds for electronic excitation of nitrogen molecules are above 6 eV and do not contribute to the evolution of the EVDF. The transport cross-section as well as the cross-sections for the vibrational excitation were taken from [28]. The initial zero-order EVDF harmonic formed by UV pulse is supposed to be characterized by the Gaussian form [22]:

$$f_0(\rho,z=ct,v) = \frac{1}{4\pi}\frac{m^{\frac{3}{2}}}{\Delta\varepsilon\sqrt{2\pi(mv^2/2)}}\times exp\left(-\frac{(mv^2/2-\varepsilon_0)^2}{\Delta\varepsilon^2}\right) \quad (17)$$

with $\varepsilon_0 = 1.87$ eV and $\Delta\varepsilon = 0.1$ eV. The last value is typical for ionization by laser pulses of femtosecond duration. We assume that angular velocity distribution in the photoelectron peak is nearly isotropic (the isotropization time is of order of the reverse transport frequency for the electrons with the energy equal to ε_0). Hence, we have the following initial condition for an anisotropic harmonic of the EVDF:

$$f_1(\rho, z = ct, v) \equiv 0. \quad (18)$$

The function $f_0(\vec{r}, v, t)$ was normalized according to the expression

$$4\pi \int f_0(\vec{r}, v, t) v^2 dv = 1. \quad (19)$$

We note that since the values of vibrational and low-level ($a\ ^1\Delta$ and $b\ ^1\Sigma$ states) electronic excitation cross sections for oxygen molecule are significantly less than the nitrogen ones it is possible to neglect them at a qualitative level of study.

The wave Equation (8) is solved jointly with the set of equations for zero—and first—order harmonics (13), (14) at each spatial grid point. The brief discussion of the numerical procedure can be found in [32] and in references therein. Similar to [18,32] the temporal step of integration is $\Delta t = 4 \times 10^{-15}$ s, step of space discretization is $\Delta z = c \times \Delta t = 1.2 \times 10^{-4}$ cm and $\Delta\rho = 0.065$ cm. The total spatial area for calculations is chosen as $\ell = 1.0$ cm and $R_{max} = 6.0$ cm. Regarding the Boltzmann equation, it is well-known that two-term expansion leads to the diffusion type equation in velocity (or energy) space. Hence, an explicit scheme for a numerical solution can be used provided that the Courant condition is fulfilled [25]. In reality in our numerical scheme, the step for integration of the Boltzmann equation is determined by the step necessary for wave equation integration.

3. Results and Discussion

3.1. Amplification in the Nonequilibrium Plasma Channel and Formation of the Unipolar THz pulses.

We will start our discussion with the analysis of the spatial pulse structure after L = 30 cm propagation in nonequilibrium nitrogen plasma channel with homogeneous electron density profile along z-axis of radius $R_0 = 1.5$ cm with radial profile given by (5) and different values of the electron density $N_e^{(0)}$ (Figure 2). In our simulations we characterize the pulse by the peak intensity value which is determined via the relation $I_0 = cE_0^2/8\pi$.

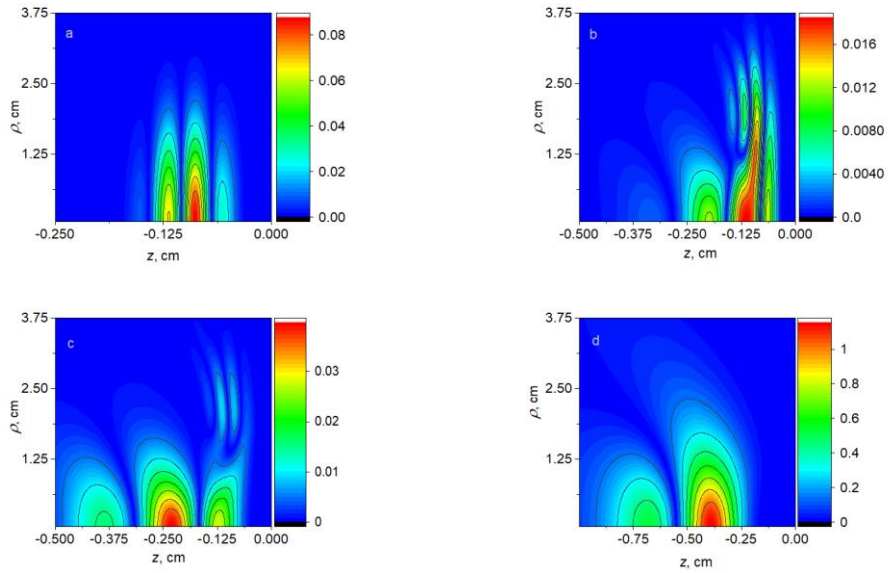

Figure 2. 3D spatial distribution of the absolute value of the electric field strength in the THz pulse: initial distribution (**a**), after the 30 cm length propagation in the nonequilibrium nitrogen plasma channel with Gaussian profile of electron density with $N_e^{(0)} = 10^{13}$ cm^{-3} (**b**) 3×10^{13} cm^{-3} (**c**) and 10^{14} cm^{-3} (**d**). Radial sizes of channel and the seed THz pulse are $R_0 = \rho_0 = 1.5$ cm. The level lines

indicate the certain values of the pulse electric field strength. The femtosecond UV pulse is located at the point $z - ct = 0$. Initial THz pulse intensity is weak and does not contribute to the EVDF evolution.

All the plots are normalized to the maximum absolute value of the seed pulse field strength. The dramatic reconstruction of the seed pulse structure is observed with the increment of electron density. Pulse structure evolution emerges in the near-axis area, while far from the axis the pulse keeps its initial form (see Figure 2b,c). We also note the effect of shifting of THz pulse spectrum to the lower frequencies followed by the pulse elongation as well as the increase of delay between the initial front of the THz pulse and leading UV. Most interesting is the fact that at high electron densities (Figure 2d) the amplified pulse is characterized by the non-zero value of the integral (3), it means the transformation of the initially bipolar pulse to the unipolar one. The physics of this transformation will be discussed below.

To obtain quantitative characteristics of the THz pulse propagation and amplification we introduce the gain at given propagation length L

$$g(L) = \int E^2(\rho, z, t = L/c)\rho d\rho dz / \int E^2(\rho, z, t = 0)\rho d\rho dz. \quad (20)$$

where the integrals are taken over the entire spatial area including $\rho > \rho_0$.

We see that for the electron density above some critical value $N_e^* \sim 4 \times 10^{13}$ cm^{-3} the gain factor is larger than the unity and exceeds $g(L = 30\ cm) \sim 1000$ for $N_e^{(0)} \cong 10^{14}$ cm^{-3} for ρ_0 =1.5 cm (see Figure 3a). For channel radius ρ_0 =1.0 cm the diffraction divergence is more significant, therefore the gain factor is lower. Below the electron density N_e^* we observe the absorption of the THz pulse energy. Such absorption occurs due to the fact that a significant part of the seed pulse spectrum is located in the range $\omega > \nu_{tr}$. As a result, the high energy spectrum part of the pulse is absorbed, while the low-energy part is not amplified enough for electron densities below the critical value. Such situation is shown in Figure 3b, where the temporal evolution of pulse spectrum for $N_e^{(0)} = 2 \times 10^{13}$ cm^{-3} indicates the dramatic spectrum reconstruction. The significant pulse amplification is accompanied by the pulse transformation to the quasi-unipolar one (see Figure 4). Similar transformation was observed for the process of amplification of a single cycle THz pulse in Xe plasma channel (see [16]), where such an effect becomes possible only for strong THz fields of the order of 10^7 W/cm^2, that are able to rapidly destroy the initial peak-like EVDF structure. The situation is quite different for the case of the nonequilibrium plasma channel in nitrogen. Due to the effective vibrational excitations of N_2 molecules in the energy range ~2–3 eV the typical time of EVDF relaxation for the plasma at atmospheric pressure is of order of several picoseconds [27]. As a result, the leading front of the THz pulse is located in the amplification zone behind the UV pulse while its trailing edge is not amplified. So, the unipolar pulses formation becomes possible for any value of the seed THz pulse intensity.

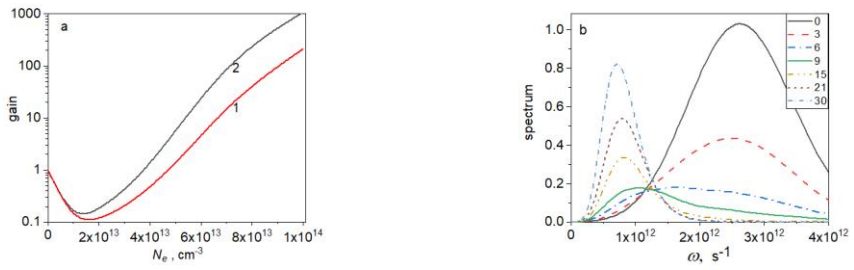

Figure 3. The gain (**a**) after 30 cm propagation in dependence on the electron density in plasma channel for initial channel and beam parameters $R_0 = \rho_0$ =1.0 cm (1) and 1.5 cm (2). The field of THz pulse is weak and does not contribute to the EVDF evolution. On-axis spectra (**b**) of the THz

pulse for different propagation lengths (given in the inset in cm) for $N_e^{(0)} = 2 \times 10^{13}$ cm^{-3} and $R_0 = \rho_0$ =1.5 cm.

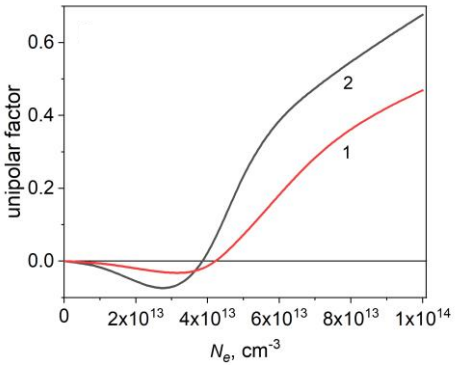

Figure 4. The unipolar factor after 30 cm propagation in dependence on electron density in the plasma channel for initial channel and beam parameters $R_0 = \rho_0$ =1.0 cm (1) and 1.5 cm (2). The field of THz pulse is weak and does not contribute to the EVDF evolution.

To provide more insight into the formation of the unipolar pulse we present on-axis EVDFs for different spatial points in the plasma channel behind the UV laser pulse (see Figure 5). As the THz pulse has low intensity these data are valid for any propagation length. One can see that for the spatial area $z \leq -0.2$ cm the EVDF peak moves from its initial position $\approx 8.0 \times 10^7$ cm/s to $\approx 7.2 \times 10^7$ cm/s. This value approximately corresponds the boundary of the region with positive derivative $d\sigma_{tr}(v)/dv > 0$ (see data in Figure 1). This fact supports our statement that only the pulse leading front can be amplified. Hence, the pulse can be transformed to the unipolar one upon its propagation.

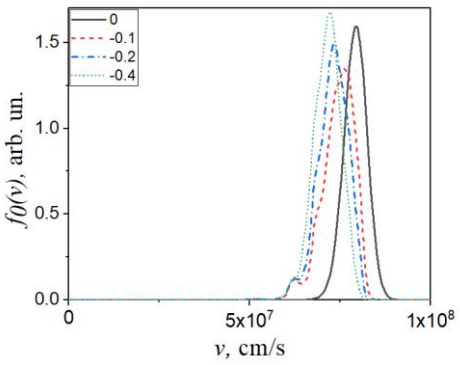

Figure 5. On-axis electron velocity distribution functions in the plasma channel for different spatial points behind the leading UV pulse. The point positions are given in the inset in centimeters. The field of THz pulse is weak and does not contribute to the EVDF evolution.

Now let us discuss the amplification and formation of unipolar pulses for the case of high energy THz pulses when the amplified THz field has significant impact on the EVDF evolution. The gain and the unipolar factor at the 30 cm propagation length for different values of initial pulse peak intensities are shown in Figure 6. Below pulse intensities 10^3 W/cm^2 the dependence of the gain versus intensity is flat, i.e., there is no influence of the amplified THz field on the EVDF. Above this value which is nearly the same for both

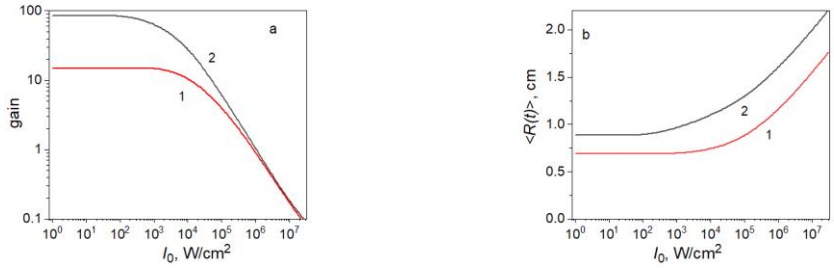

Figure 6. The gain (**a**) and the unipolar factor (**b**) in dependence on the seed pulse peak intensity for initial channel radii $R_0 = \rho_0$ =1.0 cm (1) and 1.5 cm (2), electron density is 7×10^{13}cm^{-3}.

$R_0 = \rho_0$ =1.0 cm and 1.5 cm the gain rapidly drops. For the seed pulse intensities $I_0 \geq I_0^* \approx 10^6$ W/cm^2 it becomes less than unity, i.e., the amplification is changed by the absorption. Near the value I_0^* the amplification dominantly takes place for the rising edge of the pulse, while for the trailing edge the THz energy is absorbed. As a result, there is an increase in the unipolar factor within this intensity region (see Figure 6b). The maximum possible value of the unipolar factor reaches $U \approx 0.7$ for $R_0 = \rho_0$ =1.5 cm. Thus, for considered parameters the seed bipolar pulse is not amplified but can be converted to the unipolar one.

To confirm the above conclusion in Figure 7 we present the EVDFs at different propagation lengths calculated for two spatial points behind the UV pulse for the initial pulse intensity 10^6 W/cm^2. We see that for spatial point $z - ct = -0.1$ cm there is almost no dependence of the EVDF on the propagation length, i.e., the THz field does not contribute to the EVDF evolution. On the other hand, for the spatial point $z - ct = -0.4$ cm the more the propagation length the wider the peak of the EVDF that prevents the possibility of the amplification process.

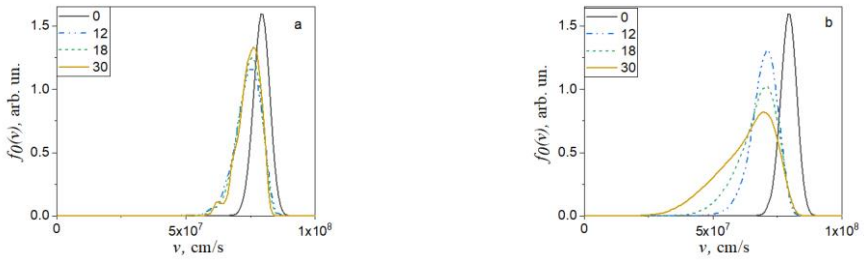

Figure 7. On-axis electron velocity distribution functions in dependence on propagation length in the spatial points behind the UV pulse $z - ct = -0.1$ cm (**a**) and -0.4 cm (**b**) for $\rho_0 = 1.5$ cm, I_0 =10^6 W/cm^2. The propagation lengths (in cm) are given in the inset.

3.2. Transferring of the Unipolar THz Pulse out of Plasma Channel

We have already mentioned that pulses with the nonzero value of the pulse electric field area (unipolar pulses) are of importance for a number of practical applications. On

the other hand, it is known that unipolar pulses do not propagate in a free space and rapidly change to the bipolar ones. For this reason, one should draw attention to the process of delivery of the THz unipolar pulse from the plasma channel to the remote target. In this section we plan to analyze the features of the unipolar pulse formed in the extended nonequilibrium plasma channel during the process of its transferring to the free space.

First, we would like to consider the sharp boundary of the plasma channel of the total length $L = 30$ cm (see Equation (6)). Such plasma density profile can be realized if the THz pulse transfers from the channel to the free space through the transparent window. Out of the channel the gas is nonionized and its permittivity is equal to unity. The dependencies of the unipolar factor on the propagation length both inside and outside of the plasma channel are plotted in Figure 8 for $R_0 = \rho_0$ =1.0 cm and 1.5 cm. Indeed, we observe that after the THz pulse transferring into free space the unipolar factor decreases. At a distance of 15 cm the *U*-factor is reduced approximately twice. It means that a target for the unipolar pulse exposure should be located rather close to the output window. The smoothing of the electron density profile (smoothing parameter $\delta = 5$ cm, see Equation (7)) does not essentially change the data obtained for the sharp profile (see Figure 8).

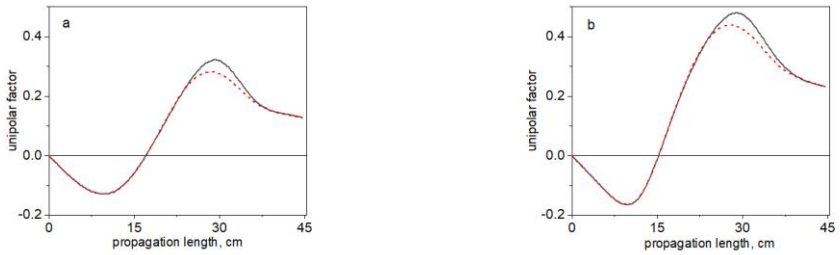

Figure 8. Unipolar factors in the dependence on the propagation length for plasma channel parameters R_0 =1.0 cm (**a**) and 1.5 cm (**b**). The boundary between the plasma channel and free space is at 30 cm. Curves correspond to rectangular (solid) and smoothed (dash) electron profiles along *z*–axis.

The detailed information on the THz pulse evolution after its transfer from the plasma channel to a free space in the case of the sharp plasma boundary is presented in Figures 9 and 10. As previously, we assume that the seed THz pulse is amplified in the plasma channel at the length $L = 30$ cm. Spatial structures of the THz field at the «plasma–free space» boundary and after the 15 cm propagation in the free space are given in Figure 9. The on-axis field distributions for the same propagation lengths are depicted in Figure 10. There are two main effects, that should be emphasized: (1) significant diffraction that increases the transverse size of the beam (see Figure 9); (2) evolution of the initial quasi-unipolar pulse back to the bipolar one (Figure 10). The unipolar factor decreases approximately twice at a distance 15 cm and undergoes further decrease at longer distances. The last process is accompanied by the formation of the extended low-level low-frequency tail that can be observed in Figure 10b.

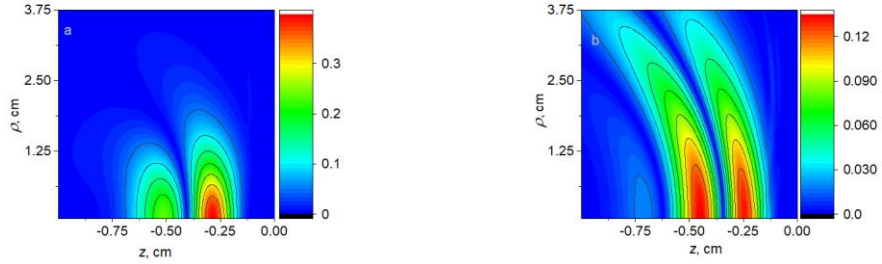

Figure 9. Spatial distribution of the absolute value of the electric field strength in the THz pulse: distribution at the «plasma–free space» boundary after the 30 cm propagation in nonequilibrium nitrogen plasma channel with Gaussian profile of electron densities with $N_e^{(0)} = 7 \times 10^{13}$ cm^{-3} (**a**), after additional 15 cm length propagation in the free space (**b**). Radial sizes of channel and THz pulse are $R_0 = \rho_0 = 1.5$ cm. The level lines indicate the certain values of pulse electric field strength. The femtosecond UV pulse is located at the point $z - ct = 0$. Initial THz pulse intensity is weak and does not contribute to the EVDF evolution.

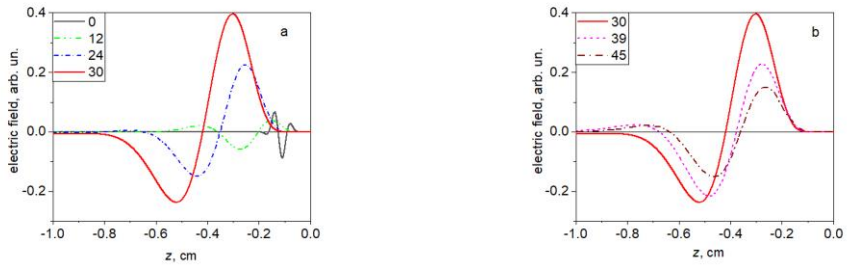

Figure 10. On-axis distributions of the electric field strength in the THz pulse inside the plasma channel (**a**) and after its propagation in the free space (**b**). Propagation lengths are given in the inset in cm. All the parameters of the plasma channel and initial pulse correspond to those given in Figure 8. The femtosecond UV pulse is located at the point $z - ct = 0$.

To conclude our discussion, we would like to note that for experimental realization of the quasi-unipolar pulse formation, we need the UV pulse of the energy about 0.5 J. Such pulses are rather close to those available at the Lebedev Physical Institute [37]. We also note that for given parameters the multiply filamentation of the UV laser pulse can be realized. If so, the radial electron density distribution will be much more complicated function of radial coordinate. On the other hand, it was demonstrated in [38] that for similar pulse parameters filaments arise at propagation lengths above 75 cm that is significantly larger than the plasma channel length in our study. The estimates of filamentation length [39] for given UV pulse parameters provide the value about 100 cm that is consistent with [38].

4. Conclusions

In summary, we develop a fully self-consistent three-dimensional model to study the terahertz pulse amplification as well as unipolarity formation in nonequilibrium nitrogen plasma channel formed by the multiphoton ionization by femtosecond UV laser pulse. In comparison with the xenon plasma channel fast relaxation of the EVDF in nitrogen plasma makes it possible to produce THz pulses with nonzero integral of the electric field strength over the pulse area for any value of the seed pulse intensity, including low intensity pulses. The problem of transferring of the unipolar pulse from the nonequilibrium plasma channel to the free space was analyzed. It was found that beyond the channel the unipolar pulse transforms to the bipolar one and a rapid diffraction divergence is observed. Hence, possible experiments on the interaction of the unipolar pulses with different microscopic objects should be conducted rather close to the output window near the boundary between a plasma channel and free space.

Author Contributions: Conceptualization, A.V.B.; Data curation, A.M.P.; Formal analysis, E.A.V.; Investigation, A.V.B.; Software, E.A.V.; Supervision, A.V.B. and A.M.P.; Writing—original draft, A.M.P.; Writing—review & editing, A.V.B. All authors have read and agreed to the published version of the manuscript.

Funding: A.V. Bogatskaya thanks the Foundation for the Advancement of Theoretical Physics and Mathematics ("Basis" foundation), Grant No. 20-1-3-40-1.

Institutional Review Board Statement: Not applicable.

Informed Consent Statement: Not applicable.

Data Availability Statement: Data underlying the results presented in this paper are not publicly available at this time, but may be obtained from the authors upon reasonable request.

Acknowledgments: The contribution of A. M. Popov to this research was performed according to the Development program of the Interdisciplinary Scientific and Educational School of MSU 'Photonic and Quantum Technologies. Digital Medicine'.

Conflicts of Interest: The authors declare no conflict of interest.

References

1. Manzoni, C.; Mucke, O.D.; Cirmi, G.; Fang, S.; Moses, J.; Huang, S.W.; Hong, K.H.; Cerullo, G.; Kartner, F.X. Coherent pulse synthesis: Towards sub-cycle optical waveforms. *Laser Photon. Rev.* **2015**, *9*, 129.
2. Hassan, M.; Luu, T.; Moulet, A.; Raskazovskaya, O.; Zhokhov, P.; Garg, M.; Karpowicz, N.; Zheltikov, A.M.; Pervak, V.; Krausz, F.; et al. Optical attosecond pulses and tracking the nonlinear response of bound electrons. *Nature* **2016**, *530*, 66–70.
3. Yoshioka, K.; Igarashi, I.; Yoshida, Sh.; Arashida, Yu.; Katayama, I.; Takeda, J.; Shigekawa, H. Subcycle mid-infrared coherent transients at 4 MHz repetition rate applicable to light-wave-driven scanning tunneling microscopy. *Opt. Lett.* **2019**, *44*, 5350–5353.
4. Arkhipov, R.; Arkhipov, M.; Pakhomov, A.; Babushkin, I.; Rosanov, N. Half-cycle and unipolar pulses (Topical Review). *Las. Phys. Lett*. **2022**, *19*, 043001.
5. Chai, X.; Ropagnol, X.; Raeis-Zadeh, S.M.; Reid, M.; Safavi-Naeini, S.; Ozaki, T. Subcycle Terahertz Nonlinear Optics. *Phys. Rev. Lett.* **2018**, *121*, 143901.
6. Arkhipov, R.; Pakhomov, A.; Arkhipov, M.; Babushkin, I.; Demircan, A.; Morgner, U.; Rosanov, N. Unipolar subcycle pulse-driven nonresonant excitation of quantum systems. *Opt. Lett.* **2019**, *44*, 1202–1205.
7. Arkhipov, R.; Pakhomov, A.; Arkhipov, M.; Demircan, A.; Morgner, U.; Rosanov, N.; Babushkin, I. Selective ultrafast control of multi-level quantum systems by subcycle and unipolar pulses. *Opt. Express.* **2020**, *28*, 17020–17034.
8. Ramasesha, K.; Leone, S.R.; Neumark, D.M. Real-time probing of electron dynamics using attosecond time-resolved spectroscopy. *Ann. Rev. Phys. Chem.* **2016**, *67*, 41.
9. Rosanov, N. On acceleration of a relativistic particle by a radiation pulse. *Opt. Spectrosc.* **2019**, *126*, 140–143.
10. Rosanov, N.; Tumakov, D.; Arkhipov, M.; Arkhipov, R. Criterion for the yield of micro-object ionization driven by few- and subcycle radiation pulses with nonzero electric area. *Phys. Rev. A* **2021**, *104*, 063101.
11. Sajadi, M.; Wolf, M.; Kampfrath, T. Transient birefringence of liquids induced by terahertz electric-field torque on permanent molecular dipoles. *Nat. Commun.* **2017**, *8*, 14963.
12. Pakhomov, A.; Arkhipov, M.; Rosanov, N.; Arkhipov, R. Ultrafast control of vibrational states of polar molecules with subcycle unipolar pulses. *Phys. Rev. A* **2022**, *105*, 043103.
13. Arkhipov, R.; Arkhipov, M.; Rosanov, N. Unipolar light: Existence, generation, propagation, and impact on microobjects. *Quantum Electron.* **2020**, *50*, 801–815.
14. You, D.; Bucksbaum, P.H. Propagation of half-cycle far infrared pulses. *J. Opt. Soc. Am. B* **1997**, *14*, 1651–1655.
15. Arkhipov, M.; Arkhipov, R.; Rosanov, N. Obtaining Unipolar Pulses at Far Field Zone of the Source. *Opt. Spectrosc.* **2021**, *129*, 1193–1195.
16. Bessonov, E.G. On a class of electromagnetic waves. *Sov. Phys. JETP* **1981**, *53*, 433.
17. Rosanov, N. Area of ultimately short light pulses. *Opt. Spectrosc.* **2009**, *107*, 721–725.
18. Bogatskaya, A.; Volkova, E.; Popov, A. Unipolar terahertz pulse formation in a nonequilibrium plasma channel formed by an ultrashort uv laser pulse. *Phys. Rev. E* **2021**, *104*, 025202.
19. Arkhipov, R.; Pakhomov, A.; Arkhipov, M.; Babushkin, I.; Tolmachev, Yu.; Rosanov, N. Generation of unipolar pulses in nonlinear media. *JETP Lett.* **2017**, *105*, 408–418.
20. Sazonov, S. Soliton-like unipolar objects in nonequilibrium dissipative media. *Laser Phys. Lett.* **2021**, *18*, 105401.
21. Shou, Y.; Hu, R.; Gong, Z.; Yu, J.; Chen, J.; Mourou, G.; Yan, X.; Ma, W. Cascaded generation of isolated sub-10 attosecond half-cycle pulses. *N. J. Phys.* **2021**, *23*, 053003.
22. Bogatskaya, A.; Volkova, E.; Popov, A. New method of unipolar THz pulse generation in photoionised xenon plasma. *Plasma Sources Sci. Technol*. **2021**, *30*, 085001.
23. Zhang, D.; Bai, Y.; Zeng, Y.; Ding, Y.; Li, Z.; Zhou, C.; Leng, Y.; Song, L.; Tian, Y.; Li, R. Towards high-repetition-rate intense terahertz source with metal wire-based plasma. *IEEE Photon. J.* **2022**, *14*, 5910605.
24. Sychugin, S.; Novokovskaya, A.; Bakunov, M. Propagation dynamics of optically generated unipolar electromagnetic pulses. *Phys. Rev. A* **2022**, *105*, 053528.
25. Bogatskaya, A.; Popov, A. On the possibility of the amplification of subterahertz electromagnetic radiation in a plasma channel created by a high intensity ultrashort laser pulse. *JETP Lett.* **2013**, *97*, 388.

26. Bogatskaya, A.; Smetanin, I.; Volkova, E.; Popov, A.M. Guiding and amplification of microwave radiation in a plasma channel created in gas by intense ultraviolet laser pulse. *Las. Part. Beams* **2015**, *33*, 17.
27. Bogatskaya, A.; Bin, H.; Popov, A.; Smetanin, I. Nonequilibrium laser plasma of noble gases: Prospects for amplification and guiding of the microwave radiation. *Phys. Plasmas* **2016**, *23*, 093510.
28. Phelps, A.; Pitchford, L. Anisotropic scattering of electrons by N_2 and its effect on electron transport. *Phys. Rev. A* **1985**, *31*, 2932.
29. Bogatskaya, A.; Volkova, E.; Popov, A. On the possibility of a short subterahertz pulse amplification in a plasma channel created in air by intense laser radiation. *J. Phys. D* **2014**, *47*, 185202.
30. Bogatskaya, A.; Volkova, E.; Popov, A. Nonequilibrium plasma channel in gaseous media formed by powerful UV laser as a waveguide for transportation and amplification of short microwave pulses. *Laser Phys. Lett.* **2015**, *12*, 035301.
31. Bogatskaya, A.; Volkova, E.; Popov, A. The response of nonequilibrium nonstationary plasma created by an intense femtosecond UV laser pulse in rare gases to the emission of the THz frequency band. *Laser Phys. Lett.* **2019**, *16*, 066008.
32. Bogatskaya, A.; Volkova, E. 3D modeling of short THz pulse propagation and amplification in the nonequilibrium plasma channel. *JOSA B* **2022**, *39*, 299.
33. Seifert, T.; Jaiswal, S.; Sajadi, M.; Jakob, G.; Winner, S.; Wolf, M.; Kläui, M.; Kampfrath, T. Ultrabroadband single-cycle terahertz pulses with peak fields of 300 kV cm−1 from a metallic spintronic emitter. *Appl. Phys. Lett.* **2017**, *110*, 252402.
34. Balčiūnas, T.; Lorenc, D.; Ivanov, M.; Smirnova, O.; Zheltikov, A.; Dietze, D.; Unterrainer, K.; Rathje, T.; Paulus, G.; Baltuška, A.; et al. CEP-stable tunable THz-emission originating from laser-waveform-controlled sub-cycle plasma-electron bursts. *Opt. Express* **2015**, *23*, 15278.
35. Ginzburg, V.; Gurevich, A. Nonlinear phenomena in a plasma located in an altering electromagnetic field. *Sov. Phys. Usp.* **1960**, *3*, 115.
36. Raizer, Yu. *Laser-Induced Discharge Phenomena*; Consultants Bureau: New York, NY, USA, 1977.
37. Zvorykin, V.D.; Goncharov, S.A.; Ionin, A.A.; Mokrousova, D.V.; Ryabchuk, S.V.; Seleznev, L.V.; Sunchugasheva, E.S.; Ustinovskii, N.N.; Shutov, A.V. Experimental capabilities of the GARPUN MTW Ti: Sapphire—KrF laser facility for investigating the interaction of subpicosecond UV pulses with targets. *Quantum Electron.* **2017**, *47*, 319.
38. Shipilo, D.E.; Panov, N.A.; Suchungasheva, E.S.; Mokrousova, D.V.; Shutov, A.V.; Zvorykin, V.D.; Ustinovskii, N.N.; Seleznev, L.V.; Savel'ev, A.B.; Kosareva, O.G.; et al. Fifteen meter long uninterrupted filaments from sub-terawatt ultraviolet pulse in air. *Opt. Express* **2017**, *25*, 25386.
39. Chekalin, S.V.; Kandidov, V.P. From self-focusing light beams to femtosecond laser pulse filamentation. *Phys. Usp*. **2013**, *56*, 123.